

1 **Title**

2 Spatial metabolomics identifies localized chemical changes in heart tissue during chronic cardiac
3 Chagas disease

4 **Short Title**

5 Spatial metabolomics of chronic cardiac Chagas Disease

6 **Authors and Affiliations**

7 Danya A. Dean^{1,2¶}, Gautham^{2,3¶}, Jair L. Siqueira-Neto⁴, James H. McKerrow⁴, Pieter C.

8 Dorrestein^{4,5,6}, Laura-Isobel McCall^{1,2,7*}

9 ¹Department of Chemistry and Biochemistry, University of Oklahoma, Norman, Oklahoma,
10 United States of America

11 ²Laboratories of Molecular Anthropology and Microbiome Research, University of Oklahoma,
12 Norman, Oklahoma, United States of America

13 ³Department of Biology, University of Oklahoma, Norman, Oklahoma, United States of America

14 ⁴Skaggs School of Pharmacy and Pharmaceutical Sciences, University of California San Diego,
15 La Jolla, California, United States of America

16 ⁵Center for Microbiome Innovation, University of California San Diego, La Jolla, California,
17 United States of America.

18 ⁶Collaborative Mass Spectrometry Innovation Center, University of California San Diego, La
19 Jolla, California, United States of America

20 ⁷Department of Microbiology and Plant Biology, University of Oklahoma, Norman, Oklahoma,
21 United States of America

22

23 * Corresponding author

24 E-mail: lmccall@ou.edu

25 ¶These authors contributed equally to this work

26

27 **Abstract**

28 Chagas disease (CD) is one of thirteen neglected tropical diseases caused by the parasite
29 *Trypanosoma cruzi*. CD is a vector-borne disease transmitted by triatomines but CD can also be
30 transmitted through blood transfusions, organ transplants and congenital transmission. While
31 endemic to Latin America, *T. cruzi* infects 7-8 million people worldwide and can induce severe
32 cardiac symptoms including apical aneurysms, thromboembolisms and arrhythmias during the
33 chronic stage of CD. However, these cardiac clinical manifestations and CD disease
34 pathogenesis are not fully understood. Using spatial metabolomics (chemical cartography), we
35 sought to understand the localized impact of infection on the cardiac metabolome of mice
36 chronically infected with two divergent *T. cruzi* strains. Our data showed chemical differences in
37 localized cardiac regions upon chronic *T. cruzi* infection, indicating that parasite infection
38 changes the host metabolome at select sites in chronic CD. These sites were distinct from the
39 sites of highest parasite burden. In addition, we identified acylcarnitines and phosphocholines as
40 discriminatory chemical families within each heart region, comparing infected and uninfected
41 samples. Overall, our study indicated overall and positional metabolic differences common to
42 infection with different *T. cruzi* strains, and identified select infection-modulated pathways.
43 These results provide further insight into CD pathogenesis and demonstrate the advantage of a
44 spatial perspective to understand infectious disease tropism.

45 **Author Summary**

46 Chagas disease (CD) is a tropical disease caused by the parasite *Trypanosoma cruzi*. CD
47 originated in South America; however, there are now 7-8 million people infected worldwide due
48 to population movements. CD is transmitted through a triatomine vector, organ transplants,
49 blood transfusions and congenital transmission. It occurs in two stages, an acute stage (usually
50 asymptomatic) and the chronic stage. Chronic stage CD presents with severe cardiac symptoms
51 such as heart failure, localized aneurysms and cardiomyopathy. Unfortunately, what causes
52 severe cardiac symptoms in some individuals in chronic CD is not fully understood. Therefore,
53 we used liquid chromatography-tandem mass spectrometry to analyze the heart tissue of
54 chronically *T. cruzi*-infected and uninfected mice, to understand the impact of infection on the
55 tissue metabolome. We identified discriminatory small molecules related to *T. cruzi* infection.
56 We also determined that regions with the highest parasite burden are distinct from the regions
57 with the largest changes in overall metabolite profile; these locations of high metabolic
58 perturbation provide a molecular mechanism to why localized cardiac symptoms occur in CD.
59 Overall, our work gives insight to chronic cardiac CD symptom development and shapes a
60 framework for novel treatment and biomarker development.

61 **Introduction**

62 Chagas disease (CD) is a parasitic disease caused by the protozoan *Trypanosoma cruzi*
63 and is one of the designated “neglected tropical diseases” [1]. *T. cruzi* is endemic to Latin
64 America and infects 7-8 million people worldwide [1]. An estimated 300,000 infections have
65 been recorded in the United States due to a large Latin American immigrant population and
66 endemic transmission [2–4]. CD is primarily transmitted through triatomine insects of the
67 *Triatoma* and *Rhodnius* genera [2]. Non-vectorial modes of transmission involve blood
68 transfusion, transplacental transmission, and food and drink contaminated with *T. cruzi* [1]. The
69 *T. cruzi* life cycle includes three main stages: epimastigotes, trypomastigotes and amastigotes. *T.*
70 *cruzi* in the insect vector undergoes transformation from trypomastigotes to epimastigotes in the
71 midgut, and then migrates to the hindgut and differentiates into infective trypomastigotes [1].
72 Upon triatomine defecation on the human host, the infective trypomastigotes enter the host
73 through scratching or rubbing of the bite wound, or through eyes and mucosal surfaces [1].
74 Following mammalian host cell infection, trypomastigotes differentiate into amastigotes, which
75 proliferate and subsequently transform into trypomastigotes [1]. CD has two disease stages:
76 acute and chronic [1,2]. The acute stage is usually asymptomatic, or presents with non-specific
77 symptoms (fever, malaise) [1,2]. 20-30% of infected individuals will then progressively develop
78 clinical manifestations of chronic CD, including cardiomegaly, cardiac arrhythmias, apical
79 aneurysms, megacolon, and megaesophagus [2]. *T. cruzi* infections are treated with either
80 benznidazole or nifurtimox; however, these treatments cause significant adverse effects to the
81 point that up to 30% of treated individuals fail to complete the full treatment course [5,6].

82 CD was previously considered to have an autoimmune etiology, but parasite persistence
83 has now conclusively been demonstrated to be required for disease pathogenesis [7]. Along with

84 parasite persistence, chronic pro-inflammatory responses, including cytokine release and CD8+
85 T cell- mediated cytotoxicity, contribute to tissue damage [8]. A heterogeneity of interacting
86 parasite-host factors, including *T. cruzi* strain, load and tissue tropism, host genetic background,
87 and mode of infection, influence the clinical outcomes of the disease [9,10]. However, CD
88 disease pathogenesis is not yet completely understood [2]. A holistic understanding of the
89 molecular pathways involved in disease progression could help identify new drug development
90 avenues and outcome-predictive biomarkers.

91 Metabolites are the final products of mRNA and protein expression and protein activity,
92 thus providing information closely linked to phenotype [11]. Metabolic pathways are druggable.
93 They also change dynamically in response to disease [12,13]. As such, an improved
94 understanding of metabolism in CD may lead to new avenues for drug development and CD
95 patient monitoring. Acute *T. cruzi*-infection affects *in vitro* and *in vivo* host metabolic pathways,
96 including decreasing mitochondrial oxidative phosphorylation-mediated ATP production [8,14–
97 16]. In addition, acute *T. cruzi*-infected mice heart tissue and plasma showed significant up- or
98 down-regulation of certain metabolic pathways, such as glucose metabolism (glucose levels
99 elevated in heart tissue and lowered in plasma over time), tricarboxylic acid cycle (TCA)
100 (decrease in select TCA metabolites in the heart tissue and a decrease in all TCA metabolites in
101 plasma), lipid metabolism (increased long-chain fatty acids in the heart tissue and the opposite in
102 plasma), and phospholipid metabolism (high accumulation of phosphocholine precursor
103 metabolites in the heart in comparison to plasma) [14]. Prior analysis of hearts from acutely-
104 infected mice also showed that cardiac metabolite profiles reflected disease severity, with
105 changes in cardiac acylcarnitines and phosphatidylcholines predictive of acute infection outcome
106 [8]. Metabolomic analysis of chronic CD has been limited to serum and gastrointestinal tract

107 samples [17][18]. Serum analysis demonstrated significant changes in amino acid and lipid
108 metabolism, particularly acylcarnitines, sphingolipids, and glycerophospholipids [17]. Analysis
109 of GI tract samples observed persistent metabolic perturbations in the oesophagus and large
110 intestine in chronic CD, including infection-induced elevation of acylcarnitines,
111 phosphatidylcholines and amino acid derivatives [18]. However, metabolic changes in the heart
112 may differ from those in the circulation or in the GI tract [14]. It is therefore essential to perform
113 metabolomic analysis of tissues collected from the heart in chronic CD. Many sudden fatalities
114 due to chronic cardiac CD are often attributed to apical aneurysms which occur at the bottom of
115 the heart [19,20]. We therefore focused on liquid chromatography-tandem mass spectrometry-
116 based metabolomic analysis of horizontally-sectioned hearts from mice chronically infected with
117 *T. cruzi* strains CL and Sylvio X10/4. These samples had previously been analyzed in terms of
118 positional differences (heart apex vs heart base), but not in the context of metabolic changes
119 associated with chronic *T. cruzi* infection [8]. Overall, we observed significant localized
120 chemical differences associated with infection, with a disconnect between parasite localization
121 and overall positional metabolic perturbations. Our data also showed infection-induced
122 variations in acylcarnitine and phosphocholine chemical families.

123

124 **Methods**

125 **Ethics statement**

126 All vertebrate animal studies were performed in accordance with the USDA Animal
127 Welfare Act and the Guide for the Care and Use of Laboratory Animals of the National Institutes
128 of Health. The protocol was approved by the University of California San Diego Institutional
129 Animal Care and Use Committee (protocol S14187).

130 ***In vivo* experimentation**

131 All *in vivo* experimentation, sample collection and qPCR analysis was conducted and
132 previously reported in [8].

133 **Metabolite extraction and UHPLC-MS/MS**

134 The two-step procedure for metabolite extraction was adapted from Want *et al* [21] and
135 was conducted in McCall *et al* [8], with “aqueous” and “organic” extracts referring to the
136 metabolites recovered from the first 50% methanol extraction and the second 3:1
137 dichloromethane-methanol extraction, respectively. UHPLC-MS/MS analysis was conducted
138 using a Thermo Scientific UltiMate 3000 Ultra High Performance Liquid Chromatography with
139 a C8 LC column and MS/MS detection on a Maxis Impact HD QTOF mass spectrometer (Bruker
140 Daltonics), as previously reported [8][21].

141 **LC-MS/MS data analysis**

142 Data processing was performed as previously reported using Optimus, July 21, 2016
143 version [8][22]. Total ion current (TIC) normalization was performed in R studio. Principal
144 coordinate analysis (PCoA) was performed on total ion current (TIC) normalized MS1 feature
145 data table using the Bray-Curtis-Faith dissimilarity metric using QIIME1 [23], for both organic
146 and aqueous extractions combined. The three-dimensional PCoA plots were visualized in
147 EMPeror [24]. Heart three-dimensional modelling was completed using ‘ili’ (<http://ili.embl.de/>)
148 [25] using a three dimensional heart model from 3DCADBrower.com
149 (<http://www.3dcadbrower.com/>).

150 Global Natural Products Social Molecular Networking (GNPS) was used to perform
151 molecular networking according to the parameters in Table 1 [26]. Cytoscape 3.7.0. was used to
152 visualize the molecular networks [27].

153 **Table 1: Global Natural Products Social Molecular Networking (GNPS) parameters.**

Parent mass	2.0 Da
MS/MS fragment ion tolerance	0.5 Da
Cosine score	0.7
Minimum matched fragment ions	6
Analog search against the library	not allowed
Network TopK	10
Maximum Connected Component Size	100
Minimum cluster size	2
Score threshold	0.7
Library search Min Matched Peaks	6
Filter precursor window	filter
Filter peaks in 50Da window	filter

154

155 Random forest analysis was performed in Jupyter Notebook using R with the number of
156 trees set to 500. Random forest classifier cutoff was based on ranked variable importance score
157 of differential metabolites in combination with unadjusted p-values<0.05 where 4 consecutive
158 non-significant unadjusted p-values defined the cutoff. FDR-corrected Mann Whitney p<0.05 for
159 all positions was also used as an alternate method to determine significant metabolite differences.

160 Venn diagrams were used to visualize the unique and common metabolites differential between
161 CL and Sylvio X10/4 infection, compared to uninfected samples, based on heart segment
162 positions, random forest classifier for all positions, and FDR-corrected Mann Whitney $p < 0.05$
163 for all positions, using <http://bioinformatics.psb.ugent.be/webtools/Venn/>.

164

165 **Data availability**

166 Metabolomics data has been deposited in MassIVE (<http://massive.ucsd.edu/>, accession
167 #MSV000080450). Molecular networks can be accessed at
168 <https://gnps.ucsd.edu/ProteoSAFe/status.jsp?task=f16bc44c3d5040d098c978823f50c68f> (all
169 samples, Aqueous extract),
170 <https://gnps.ucsd.edu/ProteoSAFe/status.jsp?task=5f8af6d62d8549358966f3896a81063a> (all
171 samples, Organic extract).

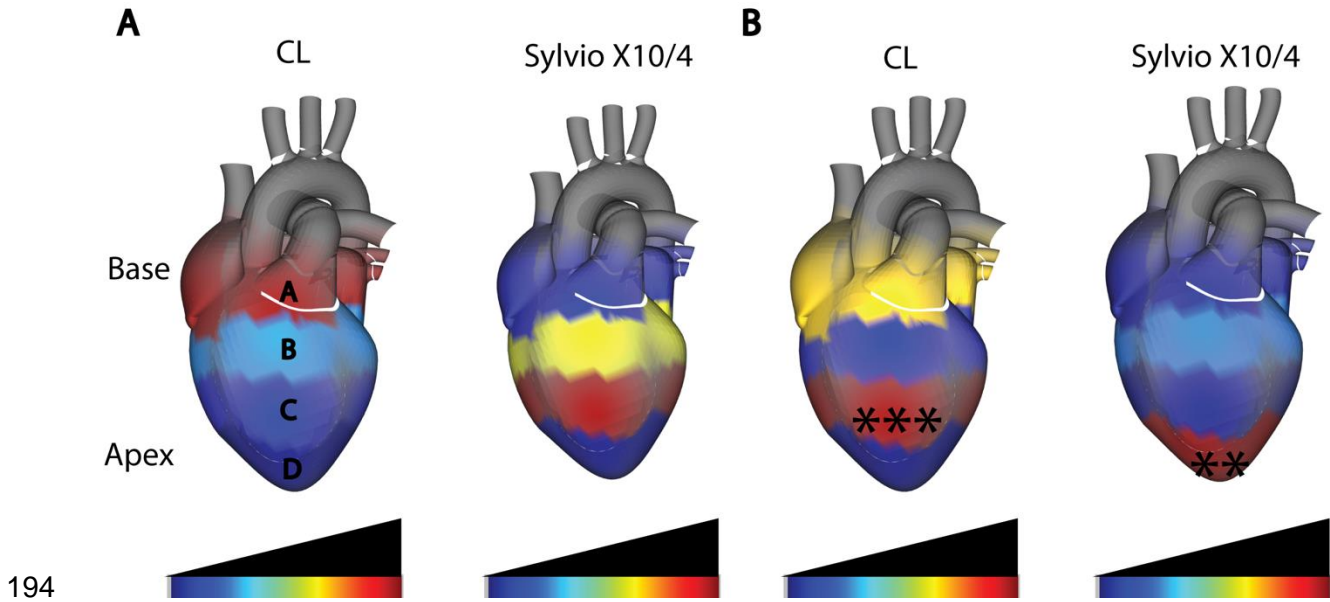
172

173 **Results**

174 The purpose of this study was to compare the metabolic impact of chronic *T. cruzi*
175 infection in the mouse heart between divergent *T. cruzi* strains and between cardiac regions. To
176 do so, we analyzed previously-collected positive mode LC-MS/MS data from mice chronically
177 infected with *T. cruzi* strain CL or Sylvio X10/4 [8]. While this prior study focused on positional
178 differences between uninfected samples and on the impact of acute infection on the cardiac
179 metabolite profile, here we specifically focused on the impact of chronic infection on the cardiac
180 metabolite profile.

181 We observed a clear distinction in the impact of *T. cruzi* infection on the overall
182 metabolite profile between *T. cruzi* strains by heart position (Fig 1, S1 figure, S2 figure). As

183 previously described [8], parasite burden was highest at the base of the heart (position A) for
184 strain CL and central positions (position C) for strain Sylvio X10/4 (Fig 1A). PERMANOVA
185 analysis indicated that the highest significant perturbation in the overall metabolite profile
186 occurred at central positions for strain CL infection (PERMANOVA analysis of Bray-Curtis-
187 Faith distance matrix $R^2=0.20813$, p-value=0.004 at position C) and at apical positions for strain
188 Sylvio X10/4 infection (PERMANOVA analysis Bray-Curtis-Faith distance matrix $R^2=0.27923$,
189 p-value=0.014 at position D) (Fig 1 B). Strikingly, in both cases chemical disturbance was
190 greatest at sites distinct from the- highest parasite burden, which corroborates our observations in
191 the context of chronic gastrointestinal *T. cruzi* infection in mice [18]. The localization of
192 chemical disturbance also provides a molecular mechanism explaining the apical aneurysms
193 observed in CD patients.



194

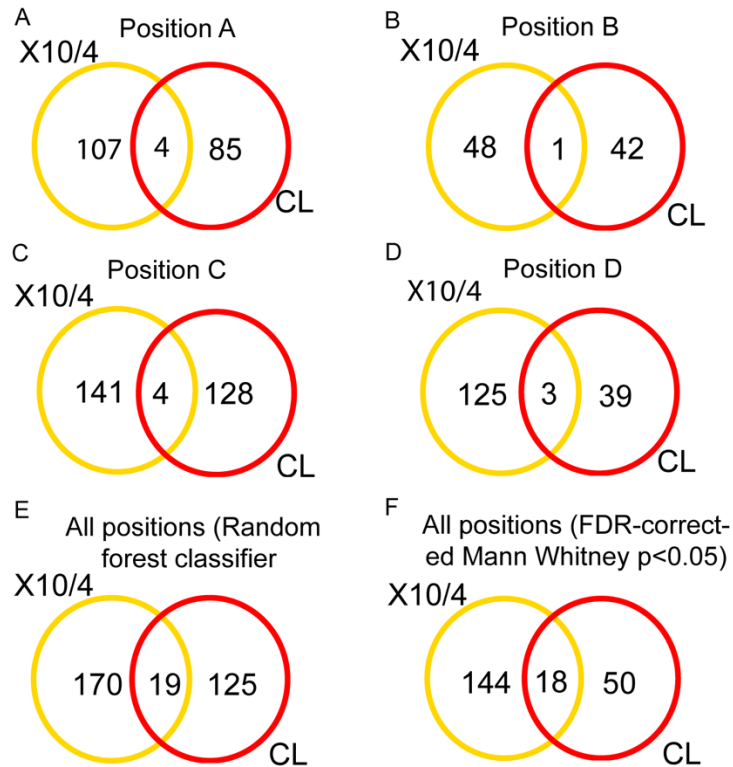
195 **Fig 1. Disconnect between sites of parasite persistence and metabolic alterations in chronic**
196 **cardiac CD.**

197 (A) Median cardiac parasite burden, as determined by qPCR. Parasite burden was highest at the
198 heart base (position A) for strain CL and central heart segments (position C) for strain Sylvio
199 X10/4, indicating parasite strain-specific differences in parasite tropism. (B) Statistically
200 significant perturbations in the overall metabolite profile between uninfected and strain CL-
201 infected (left), and between uninfected and strain Sylvio X10/4-infected mice (right) were
202 analyzed using PERMANOVA. The highest significant metabolite perturbation was at central
203 heart segments (position C) for strain CL (***, $p < 0.001$ by PERMANOVA) and at the heart
204 apex (position D) for strain Sylvio X10/4 (**, $p < 0.01$ by PERMANOVA).

205

206 To identify the specific cardiac metabolites spatially perturbed by infection, initially we
207 built a random forest classifier for each position, each strain and each extraction method,
208 comparing to uninfected matched control samples (S1-S6 tables). We first assessed the overlap
209 between the top-ranked most differential metabolites by random forest for the two different

210 strains, as described in Methods. Limited overlap of these significant metabolites was observed
211 between strains (Figure 2). However, annotation of these differential metabolites using
212 molecular networking through the GNPS platform [26] revealed that while differing in terms of
213 m/z , many were part of the same chemical families, including acylcarnitines and phosphocholine
214 (S1 - S6 Table; S3 and S4 figure).



215
216 **Fig 2. Limited overlap of specific differential metabolites between strains.**
217 Yellow and red circles represent differential metabolites between strain Sylvio X10/4-infected
218 and matched uninfected controls, and between strain CL-infected and matched uninfected
219 controls, respectively. Intersect are metabolites impacted by infection in both strains. (A-D)
220 Differential metabolites for each strain, at given heart positions. (E) Metabolites impacted by
221 infection with each strain, irrespective of position, as determined by random forest classifier,
222 with variable importance score cutoff as described in Methods. (F) Metabolites impacted by

223 infection with each strain, irrespective of heart position using FDR-corrected Mann Whitney
224 $p < 0.05$ cutoff.

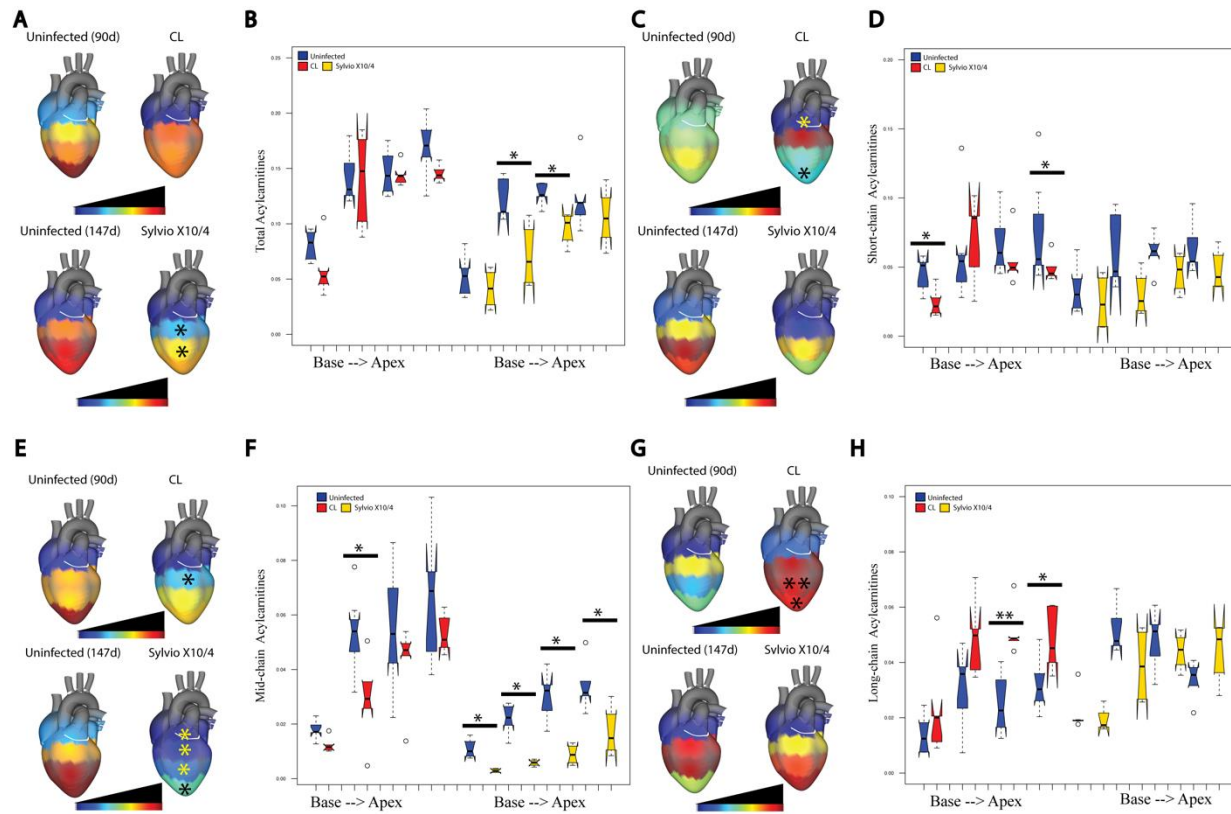
225

226 Random forest classifier identified several acylcarnitines and phosphocholines as
227 impacted by infection (S1 - S5 Tables). Both chemical families play a major role in several
228 biochemical pathways. Carnitine serves as a shuttling mechanism for fatty acids, in the form of
229 acylcarnitines, from the cytosol into the matrix of the mitochondria for beta-oxidation [28].
230 Phosphocholines are major components of lipid metabolism, cell membrane structure, and
231 choline production, the latter of which is essential for select amino acid and neurotransmitter
232 synthesis [29,30].

233 Total acylcarnitines in central positions of the heart were decreased by strain Sylvio
234 X10/4 infection compared to the uninfected group (Fig 3 A and B, Mann-Whitney $p < 0.05$). A
235 similar trend was observed for total acylcarnitines following strain CL infection when compared
236 to matched uninfected samples, even though this difference was not statistically significant (Fig
237 3A and B). Previous studies demonstrated that acylcarnitines of different lengths were associated
238 with infection outcome in acute *T. cruzi* mouse models [8]. Therefore, we sought to understand
239 how different length acylcarnitines were affected by chronic infection. Acylcarnitines are
240 classified based on the number of carbons in their fatty acid chain as short- ($\leq C4$), mid- ($C5 -$
241 $C11$), and long-chain ($\geq C12$) acylcarnitines.

242 Central and apical positions (positions B, C and D) had the largest abundance of mid and
243 long chain acylcarnitines in both CL and Sylvio X10/4 strain compared to the heart base (Mann
244 Whitney $p < 0.05$) (Fig 3 C-H). In the case of CL strain infection, when compared to uninfected
245 samples, short chain acylcarnitines were significantly decreased at the heart base and apex
246 (positions A and D, $p < 0.05$ Mann-Whitney)(Fig 3 C and D). Mid-chain acylcarnitine levels

247 were decreased by strain CL infection compared to uninfected samples at central positions
248 (position B, $p < 0.05$ Mann-Whitney) (Fig E and F). In contrast, long chain acylcarnitines were
249 significantly increased at central and apical positions (positions C and D respectively) by strain
250 CL infection (Mann-Whitney $p < 0.05$) (Fig 3 G and H). Strain Sylvio X10/4 infection
251 significantly decreased mid chain acylcarnitine at all positions (Mann-Whitney $p < 0.05$) (Fig 3 E
252 and F).



253

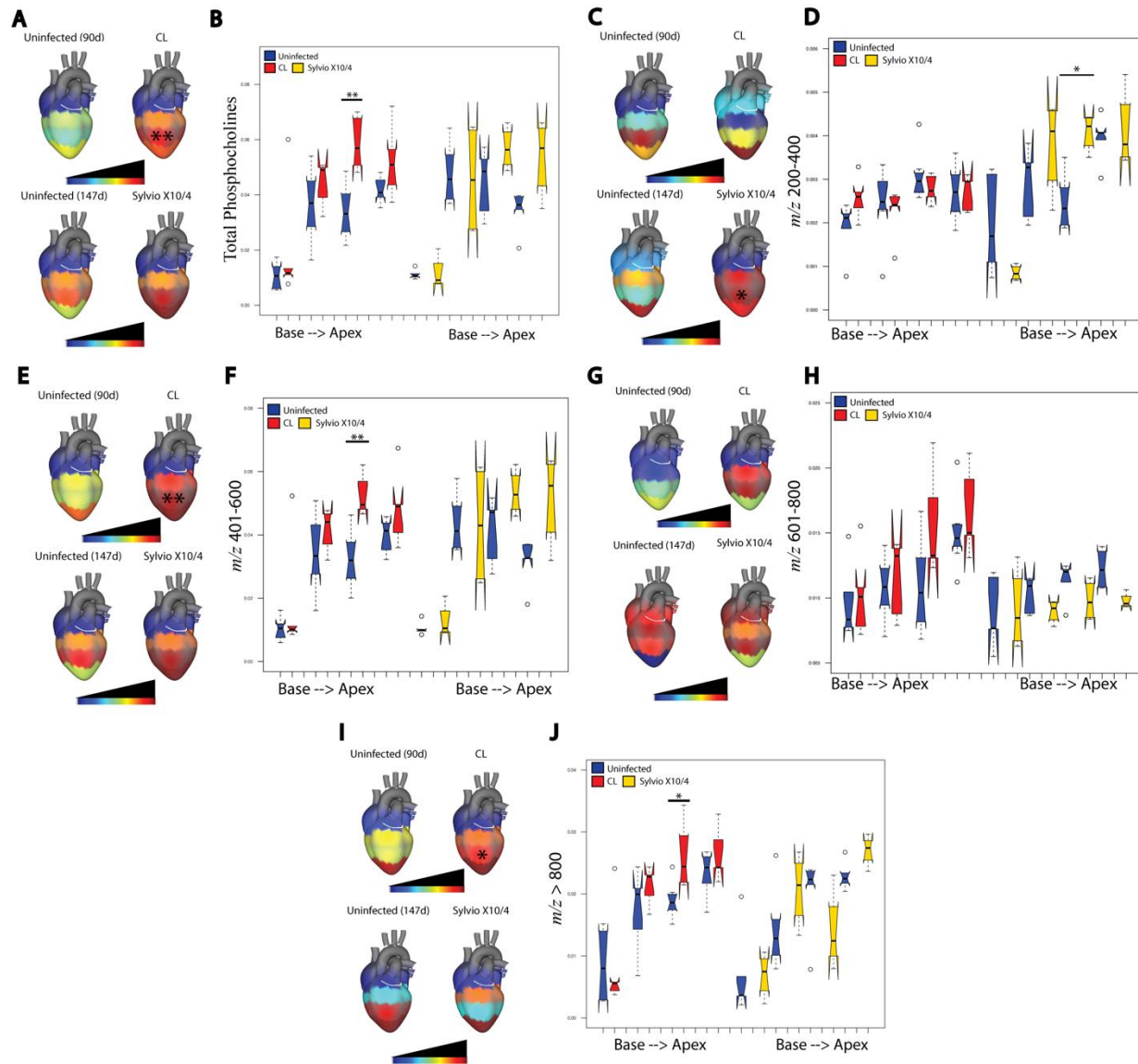
254 **Fig 3. Spatial impact of chronic *T. cruzi* infection on cardiac acylcarnitines.**

255 (A) and (B) Differential total acylcarnitine distribution between uninfected and infected heart
 256 sections for both CL and Sylvio X10/4 strains. (*, $p < 0.05$ by Wilcoxon-Mann-Whitney). (C, D)
 257 CL-infected mice showed statistically significant decreases (*, $p < 0.05$ by Mann-Whitney test) in
 258 short-chain acylcarnitine ($\leq C4$) at heart positions A and D. (E, F) Both strains of *T. cruzi*
 259 showed statistically significant decreases in mid-chain acylcarnitines. (G, H) CL-infected mice
 260 increased long-chain acylcarnitines ($\geq C12$) at position C (**, $p < 0.01$) and D (*, $p < 0.05$).

261

262 CL strain infection significantly increased total phosphocholines at central position C
 263 compared to uninfected samples (Mann-Whitney $p < 0.01$), with a similar but non-significant
 264 trend for strain Sylvio X10/4 infection at the heart apex (Fig 4 A and B). Further analysis based
 265 on phosphocholine mass was performed, because previous studies showed differences in

266 phosphocholine mass range between fatal and non-fatal acute mouse infection [8].
267 Phosphocholines were categorized into four mass ranges: short (200 - 400 m/z), mid (401 - 600
268 m/z), long (601 - 800 m/z), and very long ($>801 m/z$). Significantly elevated short
269 phosphocholines were observed in central heart positions (position C) for Sylvio X10/4 infection
270 compared to uninfected samples (Fig 4 C and D). This same pattern was also observed for CL
271 strain infection in mid and very long phosphocholines at the same position ($p < 0.01$ and < 0.05 ,
272 respectively), when compared to uninfected samples (Fig 4 E and F, I and J).



273

274 **Fig 4. Spatial impact of chronic *T. cruzi* infection on cardiac phosphocholines.**

275 (A, B) Statistically significant differences in total phosphocholine levels were identified in mice
 276 infected with CL strain at heart position C when compared to uninfected mice (**, $p < 0.01$ by
 277 Wilcoxon-Mann-Whitney test). (C,D) Sylvio X10/4-infected mice showed statistically
 278 significant differences (*, $p < 0.05$ by Wilcoxon-Mann-Whitney test) in small phosphocholines
 279 (200-400 m/z) at heart position C. (E, F) Only CL-infected mice showed statistically significant
 280 differences (**, $p < 0.01$ by Wilcoxon-Mann-Whitney test) for mid-sized phosphocholines (401-

281 600 *m/z*) at position C. (G, H) Large phosphocholines (601-800 *m/z*) were not affected by
282 infection for both strains. (I, J) CL-infected mice showed a statistically significant difference (*,
283 $p < 0.05$ by Wilcoxon-Mann-Whitney test) in very long phosphocholines (> 801 *m/z*) at position
284 C.

285 **Discussion**

286 Currently, there are 7 *T. cruzi* discrete typing units (DTUs TcI - TcVI and Tcbat). TcI to
287 TcVI are infectious to humans [31]. These DTUs, while still currently considered the same
288 species, nevertheless present significant genetic differences [31][32]. However, pathogenic
289 processes are overall similar in cardiac CD across *T. cruzi* strains, with accumulation of fibrosis
290 and inflammation, although timing and magnitude of symptoms may be different depending on
291 parasite and host characteristics [32][33]. These similarities are reflected in the common
292 metabolomic changes observed for strain Sylvio X10/4 (TcI) and strain CL (TcVI)-infected heart
293 tissue in this study, including chronic infection-induced increases in phosphocholines and
294 decreases in acylcarnitines.

295 Our results also highlight the importance of considering metabolic changes at the level of
296 chemical families, beyond just individual metabolites. While there was little overlap of highly
297 significant metabolite *m/z* at each position between strains, most differential metabolites were
298 from these two chemical families. McCall *et al.* described these two chemical families as
299 discriminatory compounds between fatal and non-fatal acute *T. cruzi* infected heart tissue [8].
300 Considering acute stage infection progresses into chronic stage infection, it is not surprising that
301 changes in the relative abundance of these molecules are also observed in chronic CD.
302 Phosphocholines have been linked to coronary heart disease due to production of
303 lysophosphatidylcholines and choline. [29,34]. Increased acylcarnitine levels have been linked to

304 cardiovascular disease as well as cardiac symptoms in those already possessing a cardiac disease
305 [35,36]. However, our results show the opposite pattern compared to non-infectious heart
306 disease, highlighting the need to specifically study CD rather than extrapolate from other cardiac
307 conditions (Fig 3). In a study addressing gene expression differences between human CD
308 cardiomyopathy and dilated cardiomyopathy, there was an upregulation of gene expression
309 associated with lipid metabolism from heart samples of human cardiac CD patients, while the
310 opposite was seen in non-infectious dilated cardiomyopathy patient samples [37]. Higher lipid
311 metabolism would increase acylcarnitine catabolism and thus decrease overall acylcarnitine
312 abundance. Decreased carnitine palmitoyltransferase and acetyltransferase levels, as observed by
313 proteomic analysis of infected mouse heart tissue [38], may alternatively also contribute to the
314 decreased acylcarnitine levels we observed.

315 Interestingly, in a study on the effects of diet on chronic *T. cruzi* mouse infection, a
316 similar pattern was observed as in our study, where serum acylcarnitines were amongst the most
317 differential compounds in infected samples compared to uninfected samples, with most short-
318 and mid-chain acylcarnitines decreased, and select long-chain acylcarnitines increased [17]. In
319 addition, significant acylcarnitine differences were seen in the gastrointestinal tract of acute *T.*
320 *cruzi*-infected mice [18]. Likewise, both long chain acylcarnitines and phospholipid synthesis
321 were increased in the heart tissue of acutely infected mice in prior studies [14]. Thus, our data
322 agree with and expand upon the existing *T. cruzi* metabolomics literature. Overall, the different
323 patterns in metabolites we observe here in contrast to other cardiac diseases is consistent with
324 differences in gene expression in humans with CD compared to other diseases.

325 Differences in pathogenesis between strains may be due to differential strain tropism.
326 Indeed, TcI strains tend to produce cardiomyopathy, while TcVI strains commonly produce

327 megacolon and megaesophagus, although cardiomyopathy can still occur [39]. Our results
328 indicate a disconnect between sites of highest parasite burden and sites of metabolic perturbation.
329 Although parasite levels were highest in central heart segments following strain Sylvio X10/4
330 infection, we observed statistically significant perturbations in metabolism at the apex of the
331 heart (Fig 1). Apical aneurysms are one of the major symptoms in chronic CD patients [40]. In
332 addition, lateral heart wall damage is also common among chronic CD patients, in central
333 regions of the heart [41], and we observed significant perturbations in cardiac metabolism at
334 lower central heart positions in strain CL infection (Fig 1B) [41]. Based on these results, we
335 propose a concept of spatial disease tolerance, whereby some tissue regions are more affected by
336 infection, while others are less functionally affected. This is likely due to a combination of host
337 and pathogen factors, given the differences we observe here between strain CL and strain Sylvio
338 X10/4 infection in the same C3H mouse genetic background. Importantly, the localization of
339 maximal metabolic perturbation in acute strain Sylvio X10/4 infection was also the heart apex,
340 indicating that the spatial course of disease may be set early in CD [8]. Likewise, host factors
341 likely contribute, such as the higher production of antiparasitic but tissue-damaging IFN γ at the
342 heart apex or specific cardiac regions being more prone to microvasculature disruptions [8].

343 These results set a foundation for biomarker studies and for host-directed therapeutic
344 development. CD may be particularly amenable to such treatment strategies, due to the
345 contribution of host-mediated tissue damage to CD pathogenesis [1,7]. Indeed, we have
346 previously shown that carnitine supplementation can be used to treat acute CD [18]. Our
347 observation of decreases in cardiac acylcarnitines in chronic CD indicate that this approach may
348 also be useful to treat chronic CD. Importantly the fact that acylcarnitines are affected in both
349 chronic CL and Sylvio X10/4 infection suggests broad applicability. Other studies have

350 emphasized the impact of metabolism modulators on CD progression. High fat diet reduces
351 parasite levels and increases survival in acute CD mouse models [42]. Treatment of acutely *T.*
352 *cruzi* infected mice with metformin (a metabolic modulator used to treat diabetic patients) also
353 led to an increase in overall survival rate and decreased p blood parasitemia [43].

354 In addition to the need for novel treatments, several studies have highlighted the
355 importance of novel diagnostic methods for CD [44,45]. Current diagnostic methods rely on
356 serological and microscopic exams and polymerase chain reaction (PCR) [46]. In addition,
357 during the chronic stage, parasite levels decrease drastically therefore PCR techniques have to be
358 used instead of microscopy. PCR however only detects the presence of infection but not cardiac
359 damage [46]. Hence, biomarkers in the form of small molecules or chemical families, as
360 identified in this study, can aid in addressing this issue. Future work will investigate whether the
361 infection-induced perturbations observed here in the heart are also detectable in clinically-
362 accessible biofluids.

363 Due to the low parasite burden in chronic Chagas disease and instrumental limits of
364 detection, we anticipate most if not all detected metabolites to be host-derived, supported by their
365 detection in uninfected tissues. As such, this study is focused on the impact of *T. cruzi* infection
366 on host metabolism. A further limitation is that many of the differential metabolites were not
367 annotatable, as is usual in metabolomic studies [47]. Nevertheless, we were able to annotate
368 metabolites affected by chronic infection that make up important host biochemical pathways.

369 Overall, our study highlights the importance of not only identifying overall differences
370 but also positional metabolic differences associated with multiple *T. cruzi* strains, and the
371 strength of systematic chemical cartography in understanding disease tropism and how it differs

372 from pathogen tropism. These results will serve as stepping stones for further CD drug
373 development and biomarker discovery, something that is urgently needed.

374 **Financial disclosure**

375 Initial sample collection was supported by a postdoctoral fellowship from the Canadian
376 Institutes of Health Research, award number 338511 to LIM (www.cihr-irsc.gc.ca/). Work in the
377 McCall laboratory at the University of Oklahoma is supported by start-up funds from the
378 University of Oklahoma (<http://www.ou.edu/>). This work was also partially supported by the US
379 National Institutes of Health (NIH) grant 5P41GM103484-07 to PCD and R21AI148886 to LIM
380 (www.nih.gov/). We further acknowledge NIH Grant GMS10RR029121 (www.nih.gov/) and
381 Bruker (www.bruker.com/) for the shared instrumentation infrastructure that enabled this work at
382 UCSD. The funders had no role in study design, data collection and analysis, decision to publish,
383 or preparation of the manuscript.

384 **References**

- 385 1. Rassi A Jr, Rassi A, Marin-Neto JA. Chagas disease. *Lancet*. 2010;375: 1388–1402.
- 386 2. Bern C. Chagas' Disease. *The New England journal of medicine*. 2015. p. 1882.
- 387 3. Beatty NL, Perez-Velez CM, Yaglom HD, Carson S, Liu E, Khalpey ZI, et al. Evidence of Likely
388 Autochthonous Transmission of Chagas Disease in Arizona. *Am J Trop Med Hyg*. 2018;99: 1534–
389 1536.
- 390 4. Gunter SM, Murray KO, Gorchakov R, Beddard R, Rossmann SN, Montgomery SP, et al. Likely
391 Autochthonous Transmission of *Trypanosoma cruzi* to Humans, South Central Texas, USA. *Emerg*
392 *Infect Dis*. 2017;23: 500–503.
- 393 5. Miller DA, Hernandez S, De Armas LR, Eells SJ, Traina MM, Miller LG, et al. Tolerance of
394 Benznidazole in a United States Chagas Disease Clinic. *Clinical Infectious Diseases*. 2015. pp.
395 1237–1240. doi:10.1093/cid/civ005
- 396 6. Forsyth CJ, Hernandez S, Olmedo W, Abuhamidah A, Traina MI, Sanchez DR, et al. Safety Profile
397 of Nifurtimox for Treatment of Chagas Disease in the United States. *Clin Infect Dis*. 2016;63: 1056–
398 1062.
- 399 7. Tarleton RL. Chagas disease: a role for autoimmunity? *Trends in Parasitology*. 2003. pp. 447–451.
400 doi:10.1016/j.pt.2003.08.008
- 401 8. McCall L-I, Morton JT, Bernatchez JA, de Siqueira-Neto JL, Knight R, Dorrestein PC, et al. Mass
402 Spectrometry-Based Chemical Cartography of a Cardiac Parasitic Infection. *Anal Chem*. 2017;89:
403 10414–10421.
- 404 9. Lewis MD, Kelly JM. Putting Infection Dynamics at the Heart of Chagas Disease. *Trends Parasitol*.

- 405 2016;32: 899–911.
- 406 10. McCall L-I, McKerrow JH. Determinants of disease phenotype in trypanosomatid parasites. Trends
407 Parasitol. 2014;30: 342–349.
- 408 11. Breitling R, Bakker BM, Barrett MP, Decuypere S, Dujardin J-C. Metabolomic Systems Biology of
409 Protozoan Parasites. Genetics Meets Metabolomics. 2012. pp. 73–84. doi:10.1007/978-1-4614-1689-
410 0_6
- 411 12. Caradonna KL, Engel JC, Jacobi D, Lee C-H, Burleigh BA. Host metabolism regulates intracellular
412 growth of *Trypanosoma cruzi*. Cell Host Microbe. 2013;13: 108–117.
- 413 13. Cestari I, Haas P, Moretti NS, Schenkman S, Stuart K. Chemogenetic Characterization of Inositol
414 Phosphate Metabolic Pathway Reveals Druggable Enzymes for Targeting Kinetoplastid Parasites.
415 Cell Chem Biol. 2016;23: 608–617.
- 416 14. Gironès N, Carbajosa S, Guerrero NA, Poveda C, Chillón-Marinas C, Fresno M. Global
417 metabolomic profiling of acute myocarditis caused by *Trypanosoma cruzi* infection. PLoS Negl Trop
418 Dis. 2014;8: e3337.
- 419 15. Knubel CP, Martínez FF, Acosta Rodríguez EV, Altamirano A, Rivarola HW, Diaz Luján C, et al. 3-
420 Hydroxy kynurenine treatment controls *T. cruzi* replication and the inflammatory pathology
421 preventing the clinical symptoms of chronic Chagas disease. PLoS One. 2011;6: e26550.
- 422 16. Garg N, Gerstner A, Bhatia V, DeFord J, Papaconstantinou J. Gene expression analysis in
423 mitochondria from chagasic mice: alterations in specific metabolic pathways. Biochem J. 2004;381:
424 743–752.
- 425 17. Lizardo K, Ayyappan JP, Ganapathi U, Dutra WO, Qiu Y, Weiss LM, et al. Diet Alters Serum
426 Metabolomic Profiling in the Mouse Model of Chronic Chagas Cardiomyopathy. Dis Markers.

- 427 2019;2019: 4956016.
- 428 18. Hossain E, Khanam S, Wu C, Lostracco-Johnson S, Thomas D, Katemauswa M, et al. 3D mapping
429 of host-parasite-microbiome interactions reveals metabolic determinants of tissue tropism and
430 disease tolerance in Chagas disease. doi:10.1101/727917
- 431 19. Jr AR, Rassi A Jr, Rassi A, Little WC. Chagas' Heart Disease. *Clinical Cardiology*. 2000. pp. 883–
432 889. doi:10.1002/clc.4960231205
- 433 20. Acquatella H. Echocardiography in Chagas heart disease. *Circulation*. 2007;115: 1124–1131.
- 434 21. Want EJ, Masson P, Michopoulos F, Wilson ID, Theodoridis G, Plumb RS, et al. Global metabolic
435 profiling of animal and human tissues via UPLC-MS. *Nat Protoc*. 2013;8: 17–32.
- 436 22. Sturm M, Bertsch A, Gröpl C, Hildebrandt A, Hussong R, Lange E, et al. OpenMS - an open-source
437 software framework for mass spectrometry. *BMC Bioinformatics*. 2008;9: 163.
- 438 23. Caporaso JG, Kuczynski J, Stombaugh J, Bittinger K, Bushman FD, Costello EK, et al. QIIME
439 allows analysis of high-throughput community sequencing data. *Nat Methods*. 2010;7: 335–336.
- 440 24. Vázquez-Baeza Y, Pirrung M, Gonzalez A, Knight R. EMPeror: a tool for visualizing high-
441 throughput microbial community data. *Gigascience*. 2013;2: 16.
- 442 25. Protsyuk I, Melnik AV, Nothias L-F, Rappé L, Phapale P, Aksenov AA, et al. 3D molecular
443 cartography using LC-MS facilitated by Optimus and 'ili software. *Nat Protoc*. 2018;13: 134–154.
- 444 26. Wang M, Carver JJ, Phelan VV, Sanchez LM, Garg N, Peng Y, et al. Sharing and community
445 curation of mass spectrometry data with Global Natural Products Social Molecular Networking. *Nat*
446 *Biotechnol*. 2016;34: 828–837.
- 447 27. Shannon P, Markiel A, Ozier O, Baliga NS, Wang JT, Ramage D, et al. Cytoscape: a software

- 448 environment for integrated models of biomolecular interaction networks. *Genome Res.* 2003;13:
449 2498–2504.
- 450 28. Longo N, Frigeni M, Pasquali M. Carnitine transport and fatty acid oxidation. *Biochim Biophys*
451 *Acta.* 2016;1863: 2422–2435.
- 452 29. Tang WHW, Wilson Tang WH, Wang Z, Levison BS, Koeth RA, Britt EB, et al. Intestinal Microbial
453 Metabolism of Phosphatidylcholine and Cardiovascular Risk. *New England Journal of Medicine.*
454 2013. pp. 1575–1584. doi:10.1056/nejmoa1109400
- 455 30. van der Veen JN, Kennelly JP, Wan S, Vance JE, Vance DE, Jacobs RL. The critical role of
456 phosphatidylcholine and phosphatidylethanolamine metabolism in health and disease. *Biochim*
457 *Biophys Acta Biomembr.* 2017;1859: 1558–1572.
- 458 31. Brenière SF, Waleckx E, Barnabé C. Over Six Thousand *Trypanosoma cruzi* Strains Classified into
459 Discrete Typing Units (DTUs): Attempt at an Inventory. *PLoS Negl Trop Dis.* 2016;10: e0004792.
- 460 32. Dorn PL, McClure AG, Gallaspy MD, Waleckx E, Woods AS, Monroy MC, et al. The diversity of
461 the Chagas parasite, *Trypanosoma cruzi*, infecting the main Central American vector, *Triatoma*
462 *dimidiata*, from Mexico to Colombia. *PLoS Negl Trop Dis.* 2017;11: e0005878.
- 463 33. Messenger LA, Miles MA, Bern C. Between a bug and a hard place: *Trypanosoma cruzi* genetic
464 diversity and the clinical outcomes of Chagas disease. *Expert Rev Anti Infect Ther.* 2015;13: 995–
465 1029.
- 466 34. Ganna A, Salihovic S, Sundström J, Broeckling CD, Hedman AK, Magnusson PKE, et al. Large-
467 scale metabolomic profiling identifies novel biomarkers for incident coronary heart disease. *PLoS*
468 *Genet.* 2014;10: e1004801.
- 469 35. Guasch-Ferré M, Zheng Y, Ruiz-Canela M, Hruby A, Martínez-González MA, Clish CB, et al.

- 470 Plasma acylcarnitines and risk of cardiovascular disease: effect of Mediterranean diet interventions.
471 Am J Clin Nutr. 2016;103: 1408–1416.
- 472 36. Strand E, Pedersen ER, Svingen GFT, Olsen T, Bjørndal B, Karlsson T, et al. Serum Acylcarnitines
473 and Risk of Cardiovascular Death and Acute Myocardial Infarction in Patients With Stable Angina
474 Pectoris. J Am Heart Assoc. 2017;6. doi:10.1161/JAHA.116.003620
- 475 37. Cunha-Neto E, Dzau VJ, Allen PD, Stamatou D, Benvenuti L, Higuchi ML, et al. Cardiac gene
476 expression profiling provides evidence for cytokinopathy as a molecular mechanism in Chagas'
477 disease cardiomyopathy. Am J Pathol. 2005;167: 305–313.
- 478 38. Wozniak JM, Silva TA, Thomas D, Siqueira-Neto JL, McKerrow JH, Gonzalez DJ, et al. Molecular
479 dissection of chagas induced cardiomyopathy reveals central disease associated and druggable
480 signaling pathways. PLoS Negl Trop Dis. 2020;14: e0007980.
- 481 39. Ramos-Ligonio A, Torres-Montero J, López-Monteón A, Dumonteil E. Extensive diversity of
482 Trypanosoma cruzi discrete typing units circulating in Triatoma dimidiata from central Veracruz,
483 Mexico. Infection, Genetics and Evolution. 2012. pp. 1341–1343. doi:10.1016/j.meegid.2012.04.024
- 484 40. Marin-Neto JA, Cunha-Neto E, Maciel BC, Simões MV. Pathogenesis of chronic Chagas heart
485 disease. Circulation. 2007;115: 1109–1123.
- 486 41. Lee-Felker SA, Thomas M, Felker ER, Traina M, Salih M, Hernandez S, et al. Value of cardiac MRI
487 for evaluation of chronic Chagas disease cardiomyopathy. Clin Radiol. 2016;71: 618.e1–7.
- 488 42. Harris EV, de Roode JC, Gerardo NM. Diet–microbiome–disease: Investigating diet's influence on
489 infectious disease resistance through alteration of the gut microbiome. PLOS Pathogens. 2019. p.
490 e1007891. doi:10.1371/journal.ppat.1007891
- 491 43. Brima W, Eden DJ, Mehdi SF, Bravo M, Wiese MM, Stein J, et al. The brighter (and evolutionarily

- 492 older) face of the metabolic syndrome: evidence from *Trypanosoma cruzi* infection in CD-1 mice.
493 *Diabetes Metab Res Rev.* 2015;31: 346–359.
- 494 44. Alonso-Padilla J, Cortés-Serra N, Pinazo MJ, Bottazzi ME, Abril M, Barreira F, et al. Strategies to
495 enhance access to diagnosis and treatment for Chagas disease patients in Latin America. *Expert Rev*
496 *Anti Infect Ther.* 2019;17: 145–157.
- 497 45. Picado A, Angheben A, Marchiol A, Alarcón de Noya B, Flevaud L, Pinazo MJ, et al. Development
498 of Diagnostics for Chagas Disease: Where Should We Put Our Limited Resources? *PLoS Negl Trop*
499 *Dis.* 2017;11: e0005148.
- 500 46. Keating SM, Deng X, Fernandes F, Cunha-Neto E, Ribeiro AL, Adesina B, et al. Inflammatory and
501 cardiac biomarkers are differentially expressed in clinical stages of Chagas disease. *Int J Cardiol.*
502 2015;199: 451–459.
- 503 47. da Silva RR, Dorrestein PC, Quinn RA. Illuminating the dark matter in metabolomics. *Proceedings*
504 *of the National Academy of Sciences of the United States of America.* 2015. pp. 12549–12550.

505 **Supporting information**

506 **S1 Table. Annotated metabolites of combined extracts perturbed by infection at**
507 **position A, identified through random forest classifier.**

508 **S2 Table. Annotated metabolites of combined extracts perturbed by infection at**
509 **position B, identified through random forest classifier.**

510 **S3 Table. Annotated metabolites of combined extracts perturbed by infection at**
511 **position C, identified through random forest classifier.**

512 **S4 Table. Annotated metabolites of combined extracts perturbed by infection at**
513 **position D, identified through random forest classifier.**

514 **S5 Table. Annotated metabolites of combined extracts perturbed by infection at**
515 **positions A-D, identified through random forest classifier.**

516 **S6 Table. Annotated metabolites of combined extracts identified as perturbed by**
517 **infection at all positions (FDR-corrected Mann Whitney $p < 0.05$).**

518 **S1 Figure. Principal coordinate analysis plot of *T. cruzi* strain CL infected (red) and**
519 **uninfected (blue) heart tissue samples. Statistically different clustering found in position C**
520 **(PERMANOVA p -value <0.05).**

521 **S2 Figure. Principal coordinate analysis plot of *T. cruzi* strain Sylvio X10/4 infected**
522 **(gold) and uninfected (blue) heart tissue samples. Statistically different clustering found in**
523 **position D (PERMANOVA p -value <0.05).**

524 **S3 Figure. Sub-molecular networks and mirror plot of aqueous and organic extract**
525 **acylcarnitines and phosphocholines.** Each pie chart is one metabolite colored by MS2 spectral
526 count in CL-infected and Sylvio X10/4-infected samples where red is CL and gold is Sylvio
527 X10/4. (A) Subnetwork of aqueous extract acylcarnitines with representative acylcarnitine mirror
528 plot (acetylcarnitine, m/z -204.124). (B) Subnetwork of aqueous extract phosphocholines with
529 representative phosphocholine mirror plot (Spectral match to 1-Hexadecanoyl-2-(9Z-
530 octadecenoyl)-sn-glycero-3-phosphocholine, m/z 758.65). (C) Subnetwork of organic extract
531 acylcarnitines with representative acylcarnitine mirror plot (acetylcarnitine, m/z - 204.126). (D)
532 Subnetwork of organic extract phosphocholines with representative phosphocholine mirror plot
533 (Spectral Match to 1-Oleoyl-2-palmitoyl-sn-glycero-3-phosphocholine, m/z -760.601).

534 **S4 Figure. GNPS mirror plots of annotated metabolites.** (A) mirror plot of m/z
535 703.575, RT 286s (top, black) to reference library spectrum (SM(d18:1/16:0), bottom, green).
536 (B) mirror plot of m/z 454.294, RT 206s (top, black) to reference library spectrum
537 (hexadecanoyl-lysophosphatidylethanolamine, bottom, green). (C) mirror plot of m/z 377.146,
538 RT 137s (top, black) to reference library spectrum (riboflavin, bottom, green). (D) mirror plot of
539 m/z 646.614, RT 417s (top, black) to reference library spectrum (ceramide, bottom, green). (E)
540 mirror plot of m/z 716.523, RT 395s (top, black) to reference library spectrum (1-palmitoyl-2-
541 oleoyl-sn-glycero-3-phosphoethanolamine, bottom, green).